https://doi.org/10.5194/hess-2020-379
Preprint. Discussion started: 18 August 2020

Hydrology and Earth System Sciences
Discussions
Open Access

At which time scale does the complementary principle perform best on evaporation estimation?

Liming Wang[1], Songjun Han[2], Fuqiang Tian[1*].

[1] Department of Hydraulic Engineering, State Key Laboratory of Hydroscience and Engineering, Tsinghua University, Beijing 100084, China

[2] State Key Laboratory of Simulation and Regulation of Water Cycle in River Basin, China Institute of Water Resources and Hydropower Research, Beijing 100038, China

Correspondence to:

Fuqiang Tian: tianfq@mail.tsinghua.edu.cn

https://doi.org/10.5194/hess-2020-379
Preprint. Discussion started: 18 August 2020

Hydrology and Earth System Sciences Discussions
Open Access
EGU

Abstract

The complementary principle has been widely used to estimate evaporation under different conditions. However, it remains unclear that at which time scale the complementary principle performs best. In this study, evaporation estimation was assessed over 88 eddy covariance (EC) monitoring sites at multiple time scales (daily, weekly, monthly, and yearly) by using the sigmoid and polynomial generalized complementary functions. The results indicate that the generalized complementary functions exhibit the highest skill in estimating evaporation at the monthly scale. The uncertainty analysis shows that this conclusion is not affected by ecosystem types nor energy correction methods. Through comparisons at multiple time scales, we found that the slight difference between the two generalized complementary functions only exists when the independent variable (x) in the functions approaches 1. The difference results in different performance of the two models at daily and weekly scales. However, such difference vanishes at monthly and annual time scales as few high x occurrences. This study demonstrates the applicability of the generalized complementary functions across multiple time scales and provides a reference for choosing the suitable timestep for evaporation estimation in relevant studies.

https://doi.org/10.5194/hess-2020-379
Preprint. Discussion started: 18 August 2020

Hydrology and Earth System Sciences Discussions

Keywords:

Evaporation; Generalized complementary functions; Multiple time scales; Ecosystem types; Energy correction methods

https://doi.org/10.5194/hess-2020-379
Preprint. Discussion started: 18 August 2020

1. Introduction

Terrestrial evaporation (*E*) including soil evaporation, wet canopy evaporation, and plant transpiration, is one of the most important components in global water and energy cycles (Wang and Dickinson, 2012). The evaporation process affects the atmosphere by a series of feedbacks on humidity, temperature, and momentum (Brubaker and Entekhabi, 1996; Neelin et al., 1987; Shukla and Mintz, 1982). Quantifying evaporation is crucial for a deep understanding of water and energy interactions between the land surface and the atmosphere. Generally, the meteorological studies focus on the evaporation change at hourly and daily scales; the hydrological applications need evaporation data at weekly, monthly or longer time scales (Morton, 1983); and the climate change researches pay more attention to the interannual variation. The observation of *E* can be operated at different time scales. For example, the Eddy covariance, lysimeter, and scintillometer can measure the evaporation at the half-hour scale, and the water balance methods can observe the evaporation at monthly to yearly scales (Wang and Dickinson, 2012). However, in most situations the observation is unavailable and the estimation of *E* is necessary. There are several types of methods for evaporation estimation, for example, the Budyko-type methods (Budyko, 1974; Fu, 1981), the Penman-type methods (Penman, 1948; Monteith, 1965) and the complementary-type methods (Bouchet, 1963; Brutsaert and Stricker, 1979). The Budyko-type methods perform well at annual or longer time scales; the Penman-type methods can be applied at hourly and daily scales; while the complementary-type methods are used at multiple time scales (Crago and Crowley, 2005; Han and Tian, 2018; Crago and Crowley, 2018; Ma et al., 2019) without an explicit cognization of the time scale issue.

Recently, the complementary principle, as one of the major types of E estimation methods, has drawn increasing attention because it can be implemented with standard meteorological data (radiation, wind speed, air temperature, and humidity) without the requirement for complicated underlying surface properties. Based on the coupling between the land surface and the atmosphere, the complementary principle assumes that the limitation of the wetness state in the underlying surface on evaporation can be synthetically reflected by the atmospheric wetness (Han et al., 2020). Bouchet (1963) first proposed the "complementary relationship" (CR), which suggested that the apparent potential evaporation (E_{pa}) and the actual E depart from potential evaporation (E_{po}) in equal absolute values but opposite directions ($E_{pa} - E_{po} = E_{po} - E$). Subsequently, the CR was extended to a linear function with an asymmetric parameter (Brutsaert and Parlange, 1998). Further studies found that the linear function underestimates E in arid environments and overestimates E in wet environments (Han et al., 2008; Hobbins et al., 2001; Qualls and Gultekin, 1997). To address the issue, Han et al. (2011; 2012; 2018) proposed a sigmoid generalized complementary function (SGC, see equation (1) for detail). As a modification to the AA approach, the SGC function illustrates the relationship between two dimensionless terms, E/E_{pen} and E_{rad}/E_{pen}, where E_{pen} is the Penman evaporation (Penman, 1948) and E_{rad} is the radiation term of E_{pen}. The SGC function shows higher accuracy in estimating E (Han and Tian, 2018; Ma et al., 2015b; Zhou et al., 2020) and outperforms the linear functions, especially in dry desert regions and wet farmlands (Han et al., 2012). Obtaining the impetus from Han et al. (2012), Brutsaert (2015) proposed a quartic polynomial generalized complementary function (PGC, see equation (5) for detail). The PGC function describes the relationship between E/E_{pa} and E_{po}/E_{pa}, where E_{pa}

and E_{po} are formulated in the manner of the AA approach. The PGC function has also been frequently used in recent years (Brutsaert et al., 2017; Hu et al., 2018; Liu et al., 2016; Zhang et al., 2017).

The prerequisite of the complementary principle is the adequate feedback between the land surface and the atmosphere, which results in an equilibrium state. In this situation, the wetness condition of the land surface can be largely represented by the atmospheric conditions. Therefore, the time scales used in the complementary principle need to satisfy the adequate feedback assumption. However, this issue involves the complex processes of atmospheric horizontal and vertical motion, and it is difficult to be explained theoretically. Morton (1983) noticed this problem earlier and suggested that the complementary principle is not suitable for short time scale (e.g., less than 3 days) mainly because of the potential lag times associated with the response of energy and water vapor storage to disturbances in the atmospheric boundary layer. However, there is no solid evidence or theoretical identification to support this inference. The original complementary relationship and the AA function are not limited by the applicable time scales. In the derivation of the advanced generalized complementary functions (SGC of Han and Tian (2018) and PGC of Brutsaert (2015)), no specific time scale is defined neither. In practice, the complementary principle has been widely adopted to estimate E at multiple time scales including hourly (Crago and Crowley, 2005; Parlange and Katul, 1992), daily (Han and Tian, 2018; Ma et al, 2015b), monthly (Ma et al, 2019; Brutsaert, 2019), and annual scales (Hobbins et al., 2004). The accuracy of the results varied in different studies. Crago and Crowley (2005) found the linear complementary

https://doi.org/10.5194/hess-2020-379
Preprint. Discussion started: 18 August 2020

function performs well in estimating E at small time scales less than half-hour using the data from several famous experimental projects (e.g., International Satellite Land Surface Climatology Project). The correlation coefficient between simulated E and observed E ranges from 0.87 to 0.92 in different experiments. The results of Ma et al. (2015b) indicated that the SGC function (RMSE = 0.39 mm day^{-1}) is competent in estimating E in an alpine steppe region of the Tibetan Plateau at the daily scale. Han and Tian (2018) applied the SGC function on the daily data of 20 EC sites from the FLUXNET and found it performs well in estimating E with a mean Nash-Sutcliffe efficiency (NSE) value of 0.66. Crago and Qualls (2018) evaluated the PGC function and their rescaled complementary functions using the weekly data of 7 FLUXNET sites in Australia, and the results showed that all the functions perform adequately with a correlation coefficient between simulated E and observed E higher than 0.9. Ma et al. (2019) also validated an emendatory polynomial complementary function at the monthly scale, and the NSE values of 13 EC sites in China are higher than 0.72. At the annual scale, Zhou et al. (2020) found the mean NSE of the SGC function is 0.28 for 15 catchments in the Loess Plateau. Since these results were derived with different functions under varied conditions, it is difficult to determine at which time scale the performance is the best, and it is more difficult to explain theoretically how long the land-atmosphere feedback needs to achieve equilibrium.

In previous studies, the model validations were mostly completed at daily scale (Brutsaert, 2017; Han and Tian 2018; Wang et al. 2020), and the datasets of evaporation estimation were often established at monthly scale (Ma et al., 2019; Brutsaert et al., 2019). However, each

https://doi.org/10.5194/hess-2020-379
Preprint. Discussion started: 18 August 2020

study only focused on a single timescale. In this study, we assessed the performance of the complementary functions on evaporation estimation at multiple time scales (daily, weekly, monthly, and yearly). The assessment was carried out over 88 EC monitoring sites with > 5-year-long observation records. In view of the fact that the complementary principle has developed to the nonlinear generalized forms, we selected two nonlinear complementary functions in the literature, i.e., the SGC function (Han et al., 2012; 2018) and the PGC function (Brutsaert, 2015). The key parameters of the complementary functions need to be determined by calibration. We chose the uniform database and the uniform parameter calibration method for the optimization of the two complementary functions. We aimed to determine the most suitable timescale for the complementary functions through comparison of the performances at different timescales. It's important not only for the deep understanding of the application of the complementary principle, but also for the timestep selection in the evaporation database establishment and evaporation trend analysis.

This paper is organized as follows. Section 1 briefly describes the development of the complementary theory and our motivations to investigate the timescale issue. Section 2 describes the two functions, the parameter calibration method, and the data sources and processing. Section 3 shows and discusses the performance of the complementary functions at multiple time scales, the dependence of the key parameters on time scales, and the uncertainties in the analysis. The conclusions are given in Section 4.

2. Methodology

2.1 The sigmoid generalized complementary function

Han et al. (2012; 2018) proposed a generalized form of the complementary function that expresses E/E_{pen} as a sigmoid function (SGC) of E_{rad}/E_{pen}:

$$y = \frac{E}{E_{Pen}} = \frac{1}{1 + m\left(\frac{x_{max} - x}{x - x_{min}}\right)^{n}}$$

$$x = \frac{E_{rad}}{E_{Pen}} \tag{1}$$

where x_{max} corresponds to the certain maximum value of x under extremely wet environments, and x_{min} corresponds to the certain minimum value of x under extremely arid environments. In this study, x_{max} and x_{min} were set as 1 and 0, respectively, for convenience. The E_{pen} term is defined by Penman's equation (Penman, 1950; Penman, 1948), which can be expressed as

$$E_{pen} = \frac{\Delta(R_n - G)}{\Delta+\gamma} + \frac{\rho c_p}{\Delta+\gamma}\frac{\kappa^2 u}{ln(\frac{z-d_0}{z_{0m}})\, ln(\frac{z-d_0}{z_{0v}})}(e_a{}^{*} - e_a) \tag{2}$$

where, Δ (kPa C^{-1}) is the slope of the saturation vapor curve at air temperature; R_n is the net radiation; G is the ground heat flux; γ (kPa C^{-1}) is a psychrometric constant; ρ is the air density; c_p is the specific heat; $\kappa = 0.4$ is the von Karman constant; u is the wind speed at measurement height; $e_a{}^{*}$ and e_a are the saturated and actual vapor pressures of air, respectively; z is the measurement height (Table S1); d_0 is the displacement height; z_{0m} and z_{0v} are the roughness lengths for momentum and water vapor, respectively, which are estimated from the canopy height (h_c, Table S1), $d_0 = 0.67h_c$, $z_{0m} = 0.123h_c$, and $z_{0v} = 0.1z_{0m}$ (Monin and Obukhov, 1954; Allen et al., 1998). E_{rad} is the radiation term of the Penman evaporation:

$$E_{rad} = \frac{\Delta(R_n - G)}{\Delta+\gamma} \tag{3}$$

The two parameters m and n of equation (1) can be determined by the Priestley-Taylor coefficient α and the asymmetric parameter b (Han and Tian, 2018).

$$\begin{cases} n = 4\alpha(1+b^{-1})x_{0.5}(1-x_{0.5}) \\ m = (\frac{x_{0.5}}{1-x_{0.5}})^{n} \end{cases} \tag{4}$$

where, $x_{0.5}$ is a variable that corresponds to $y = 0.5$, and equals to $\frac{0.5+b^{-1}}{\alpha(1+b^{-1})}$.

2.2 The polynomial generalized complementary function

Brutsaert (2015) proposed the polynomial generalized complementary (PGC) function, which describes the relationship between E/E_{pa} and E_{po}/E_{pa}. According to the AA approach (Brutsaert and Stricker, 1979), E_{pa} is formulated by Penman's (1948) equation (E_{pen}), and E_{po} is formulated by Priestley-Taylor's (1972) equation ($E_{PT} = \alpha\ E_{rad}$). We uniformed the independent variable as E_{rad}/E_{pen} to compare the two functions conveniently, and the polynomial function can be expressed as:

$$y = (2-c)\alpha^2x^2 - (1-2c)\alpha^3x^3 - c\alpha^4x^4 \tag{5}$$

where, c is an adjustable parameter. When $c = 0$, equation (5) reduce to

$$y = 2\alpha^2x^2 - \alpha^3x^3 \tag{6}$$

2.3 Parameter optimization method

In this study, α was calculated by the mean value of E/E_{rad} whenever E/E_{pen} is larger than 0.9 (Kahler and Brutsaert, 2006; Ma et al., 2015a). When all the E/E_{pen} values are less than 0.9, α was set as the default value of 1.26. The key parameter b in SGC was calibrated by an optimization algorithm with the objective function as minimization the mean absolute error (MAE) between the estimated E (by equation (1)) and the observed E. Similarly, the key parameter *c* in PGC was calibrated by an optimization algorithm with the objective function as minimization the MAE between the estimated *E* (by equation (5)) and the observed *E*.

2.4 Data sources and data processing

The eddy flux data analyzed in this study were obtained from the FLUXNET database (http://fluxnet.fluxdata.org, Baldocchi et al., 2001). Observations from a total of 88 sites around the world were analyzed. The detailed information on these sites is listed in Table S1. These sites were selected from the FLUXNET database because they have observations for longer than 5 years. The 88 sites include 11 IGBP (International Geosphere-Biosphere Programme) land cover classes: ENF, evergreen needleleaf forests (27 sites); EBF, evergreen broadleaf forests (8); DBF, deciduous broadleaf forests (13); MF, mixed forests (5); OSH, open shrublands (4); CSH, closed shrublands (1); WSA, woody savannas (3); SAV, savannas (4); GRA, grasslands (15); CRO, croplands (6); WET, permanent wetlands (2). The climate of the 88 sites ranges from arid to humid. Among the 88 sites, 11 sites have mean annual precipitation lower than 200 mm, 47 sites have precipitation between 200 ~ 500 mm and 30 sites have precipitation above 500 mm. Eleven sites are located in the Southern Hemisphere (i.e., Australia, Brazil, and South Africa) and the others are located in the Northern Hemisphere.

Variables including net radiation, sensible heat flux, latent heat flux, ground heat flux, wind speed, air temperature, air pressure, precipitation, relative humidity, and vapor pressure deficit were acquired from the daily, weekly, and monthly datasets on the FLUXNET website. We analyzed the observations in the growing seasons from April to September for the Northern Hemisphere and from October to March for the Southern Hemisphere. These study periods were selected to avoid the high biases caused by the small solar radiation or the extremely low evaporation (≈ 0) during the nongrowing season. The seasonal and annual data were acquired by averaging the monthly data of the growing seasons. Following Ershadi et al. (2014), the energy residual corrected latent heat fluxes were used, which means the residual term in energy balance is attributed to the latent heat to force the energy balance closure. To investigate the influence of different residual correction methods, the Bowen ratio energy balance method was also adopted in the uncertainty analysis. In the Bowen ratio method, the residual term is attributed into sensible heat and latent heat by preserving Bowen ratio (Twine et al., 2000). The latent heat, sensible heat, and available energy ($R_n - G$) were restricted to positive values (Han and Tian, 2018). The energy balance residual (W m^{-2}) and energy balance closure ratio for each site are shown in Table S1.

The Nash-Sutcliffe efficiency (NSE, Legates and McCabe, 1999) is used to evaluate the efficiency of estimating E by the two generalized complementary functions:

$$\mathrm{NSE} = 1 - \frac{\sum(E-E_{est})^2}{\sum(E-\bar{E})^2} \tag{7}$$

where, E_{est} (W m^{-2}) is the estimated evaporation according to equation (1) or equation (5) and $\bar{E}$ is the mean value of E (W m^{-2}).

3. Results and discussion

3.1 Performance of the SGC function at multiple time scales

https://doi.org/10.5194/hess-2020-379
Preprint. Discussion started: 18 August 2020

The relationship between the estimated E_{est} (site mean values) based on the SGC function (equation (1)) and the observed E of the 88 sites at multiple time scales is shown in Figure 1. The regression equations and determination coefficients (R^2) were calculated by the site mean results. Each dot in Figure 1 represents the site mean result averaged by daily (Figure 1a), weekly (Figure 1b), monthly (Figure 1c), and yearly (Figure 1d) results, and the total observation number is 88 (sites) at each timescale. Most of the results lie near the 1:1 line, and all the regression slopes are close to 1 with high R^2 (0.95 ~ 0.99), which means the sigmoid function exhibits good performance to estimate E at multiple time scales. The interceptions range from −1.69 to 2 W m^{-2}. All the coefficients of the regression show indistinctive differences at different time scales. However, the evaluation merits show that the performance varies at each time scale. The mean results of NSE_H, R^2_H, and $RMSE_H$ (the subscript H corresponds to the sigmoid function proposed in Han and Tian, 2018) of these sites are shown in Table 1. R^2_H represents the mean value averaged by the determination coefficients within each site. When the timescale changes from day to month, the mean NSE_H increases from 0.33 to 0.55, and R^2_H also increases from 0.61 to 0.75 (Table 1). However, they both decrease at the annual scale (NSE = 0.18 and R^2_H = 0.61). These results indicate that the SGC function exhibit the highest skill at the monthly scale. We inferred that there is a tradeoff between the random error and the number of observations. $RMSE_H$ values decrease from 24.56 W m^{-2} at the daily scale to 7.33 W m^{-2} at the annual scale, which means the random error decrease as time scale increases. At the same time, the fewer observations at the annual scale result in decreased variabilities of x and y, which affect the performance of the SGC function. On the other hand, Morton (1983) did not suggest using the complementary principle for short time intervals (e.g., less than 3 days), mainly considering the lag times associated with heat and water vapor change in the atmosphere, which can explain that the weekly and monthly results are better than the daily results.

In previous studies, the SGC function was mainly applied at the daily scale. For example, the results of Ma et al. (2015b) in the alpine steppe region showed that the NSE of the sigmoid function is 0.26 at the daily scale, which is lower than our mean value in the grassland (0.73 ± 0.08). The RMSE (11.06 W m^{-2}) is smaller than ours (16.36 ± 1.48 W m^{-2}). The mean NSE of 20 EC sites from the FLUXNET is 0.66 at daily scale in Han and Tian (2018), about two times of the result in this study, and the RMSE (18.6 ± 0.94 W m^{-2}) is lower than our mean result of 88 sites (24.56 ± 0.95 W m^{-2}).

The SGC function for the five selected sites of different ecosystem types is shown in Figure 2 to show the performance at multiple time scales (red lines in Figure 2). These five EC monitoring sites were selected because they have long-period observations (> 10 years). The five sites include an evergreen needle forest (CA-TP1, Figures 2(a) to (d)), a deciduous broad forest (US-UMB, Figures 2(e) to (h)), a woody savanna (US-SRM. Figures 2(i) to (l)), a cropland (US-Ne2, Figures 2(m) to (p)) and a grassland (US-Wkg, Figures 2(q) to (t)). As observations decrease from daily to annual scale, the results converge on the middle part of the sigmoid curves and lie closer to the fitted lines. For some sites, the annual results concentrate on a narrow range with lower annual variabilities (e.g., Figures 2(h), 2(l) & 2(t)). Generally, the key parameter (*b*) of the SGC function at these sites increases from the daily scale to the annual scale, which indicates the sigmoid curves in the two-dimensional space of E_{rad}/E_{pen}-E/E_{pen} move upwards. The detailed discussion about the variation of the parameters is elaborated in Section 3.4.

3.2 Performance of the PGC function at multiple time scales

The relationship between the estimated E_{est} (site mean values) based on the PGC function (equation (5)) and the observed E of the 88 sites at multiple time scales is shown in Figure 3. The slopes of the regression increase from 0.9 to 1 as the timescale changes from day to month, and further increase to 1.01 at the annual scale. The intercept terms decrease from 13.06 W m^{-2} at the daily scale to 0.01 W m^{-2} at the monthly scale, and further decrease to −0.25 W m^{-2} at the annual scale. The R^2 values increase from 0.83 to 0.99 as time scale increases. These coefficients of the regression show that the PGC function exhibit the highest skill at the monthly scale. The mean values of NSE_B, R^2_B, and $RMSE_B$ (the subscript B corresponds to the polynomial function proposed in Brutsaert, 2015) of these sites are shown in Table 1. When the timescale changes from day to month, NSE_B increases from 0.19 to 0.50, and R^2_B increases from 0.61 to 0.75. They decrease at the annual scale (NSE = 0.25 and R^2_H = 0.63). Again, these evaluation merits indicate that the PGC function also exhibits the highest skill at the monthly scale, which is the same as the SGC function.

The PGC function has been applied at multiple time scales in previous studies. Zhang et al. (2017) evaluate the performance of the PGC function in estimating evaporation at 4 EC flux sites located across Australia, and their results showed that the mean RMSE (24.67 W m^{-2})

https://doi.org/10.5194/hess-2020-379
Preprint. Discussion started: 18 August 2020

and R^2 (0.65) are close to our results (RMSE = 26.83 ± 1.16 W m^{-2} and R^2 = 0.61) at the daily scale. In Crago and Qualls (2018), the mean RMSE of 7 EC sites at the weekly scale is 20.6 W m^{-2} and the mean R^2 is 0.81, which are close to our mean results (RMSE = 19.17 ± 0.95 W m^{-2} and R^2 = 0.7).

The PGC functions for the five selected sites are also shown in Figure 2 (green lines). The fitted lines almost duplicate with those of SGC function in most situations when x is not too high. However, they diverge from each other when x becomes larger. Finally, y exceeds 1 when x is larger than $1/\alpha$. Generally, the key parameter (c) of the PGC function at these sites decreases from daily scale to annual scale, which also indicates the fitted curves move upwards.

3.3 Performance comparison of the SGC and PGC functions

The results of the 88 sites (Figure 1, Figure 3 and Table 1) show that the performance of the two functions are similar at monthly and annual time scales, while the SGC function performs slightly better than the PGC function at daily and weekly time scales. According to the results in Figure 2, it can be recognized that the two functions with calibrated parameters are approximately identical under non-humid environments, but their difference increases as x (E_{rad}/E_{pen}) increases. At daily and weekly time scales, quite a few ecosystems can produce very high E_{rad}/E_{pen}. Specifically, 63 of the 88 sites have high E_{rad}/E_{pen} ($x > 1/\alpha$) at the daily scale and 24 sites have high values at weekly scale. However, there are only 3 sites with $x > 1/\alpha$ at the monthly scale and no site at the yearly scale. For the SGC function, in super humid

https://doi.org/10.5194/hess-2020-379
Preprint. Discussion started: 18 August 2020

conditions, the upper part of the sigmoid curve is nearly flat and closer to the observations (e.g., Figures 2 (a), (m) & (n)). However, for the PGC function, theoretically it cannot be applied when x is over $1/\alpha$ because the estimated E_{est} will be higher than E_{pen} which is irrational. Thus, the sigmoid function performs slightly better at daily and weekly time scales. But the difference vanished at the monthly scale as few high E_{rad}/E_{pen} occurrences.

According to the results, the performance of the PGC function acts more sensitive to the timestep than that of the SGC function. On one hand, the regression relationship between E_{est} and the observed E of the 88 sites shows the performance of the SGC function remains more stable (Figure 1), while the regression results of the PGC function have higher variation when the time scale changes (Figure 3). On the other hand, the estimation merits (Table 1) further confirm the sensitivity of the PGC function. From daily scale to monthly scale, the increase of NSE_H is 0.22, while the increase of NSE_B is 0.31; $RMSE_H$ decreases by 11.36 W m^{-2} (46%) and $RMSE_B$ decrease by 13.13 W m^{-2} (49%). At the daily scale, quite a few ecosystems (63 of 88 sites) can experience frequent high E_{rad}/E_{pen} ($> 1/\alpha$) occurrences, and the PGC function does not have the ability to simulate E accurately in this situation ($E_{est} > E_{pen}$) resulting in lower efficiency. As time scale increases, the results converge on the middle part of the fitted line and the number of high x greatly reduces (Figure 2). Thus, the efficiency of the PGC function increases obviously. It's the reason that the polynomial function acts more sensitive to the timestep.

3.4 Dependence of the key parameters of the SGC and PGC functions on time scales

https://doi.org/10.5194/hess-2020-379
Preprint. Discussion started: 18 August 2020

The key parameters of the two complementary functions (*b* of the SGC function and *c* of the PGC function) vary at multiple time scales (Figure 2). To explore their changes, the values of 1/*b* and *c* of the 88 sites were averaged at each timescale. To take account of the situation that *b* is equal to infinity, we used 1/*b* instead of *b* in this analysis. Figure 4 shows the change of the two complementary functions with varied parameters at multiple time scales. The averaged 1/*b* decreases from 0.45 ± 0.05 at the daily scale to 0.24 ± 0.03 at the annual scale (Figure 4a), and the averaged *c* decreases from 0.98 ± 0.19 at the daily scale (Figure 4b) to −0.37 ± 0.22 at the annual scale. The sign of *c* changes from positive to negative at the monthly scale.

We showed the histogram of 1/*b* and *c* at multiple time scales in Figure 5 and Figure 6, respectively. At the daily scale, half of the 1/*b* values are lower than 0.3 and the mean value is 0.45 ± 0.05. At the weekly scale, the peak of the distribution moves left, nearly half of the 1/*b* values are lower than 0.2 with the mean value of 0.36 ± 0.04. At the monthly scale, the mean value is 0.29 ± 0.04 and the 1/*b* values continue to decrease. At the annual scale, the mean value decreases to 0.24 ± 0.03 and 61% of the 1/*b* values are lower than 0.2. According to Figure 6, at the daily scale, *c* follows a normal distribution (p-value = 0.17, Kolmogorov-Smirnov test) with the mean value of 0.98 ± 0.21. Nearly 1/3 of the *c* values are lower than 0. At the weekly scale, the center of the distribution moves left with the mean value of 0.43 ± 0.24. Half of the *c* values are lower than 0. At the monthly scale, the mean value is −0.04 ± 0.23, and 58% of the *c* values are lower than 0. At the annual scale, the mean value decreases to −0.37 ± 0.25, and 63% of the *c* values are lower than 0. These results support our

https://doi.org/10.5194/hess-2020-379
Preprint. Discussion started: 18 August 2020

Hydrology and Earth System Sciences
Open Access
EGU
Discussions

conclusion that $1/b$ and c decrease as time scale increases. Generally, the distribution of $1/b$ and c also move left within each ecosystem type according to Figures 5 and 6.

The reduction of $1/b$ and c indicate the curves of the complementary functions move upwards as time scale increases. Under non-humid conditions, the sigmoid function is a concave function, which means:

$$\frac{1}{2}[f(x_1) + f(x_2)] > f(\frac{x_1 + x_2}{2}) \quad (8)$$

where, f is the concave function, and x_1 and x_2 represent any two values on the x-axis. Since most of the results follow the fitted line, the averaged results of longer timestep will go upwards in the two-dimensional space of E_{rad}/E_{pen}-E/E_{pen}, so does the new fitted curve. Although under the super humid condition, the SGC function is a convex function, there is fewer data in this condition as time scale increases and the shape of this part is almost unchanged (Figure 4a). As for the PGC function, when x is in the range of 0 to $1/\alpha$, most part of it is a concave function. For example, in the situation that c is equal to 0, the second derivative is higher than 0 as long as x is lower than 2/3.

Furthermore, we found that the two key parameters, b and c present a significant correlation, indicating the two functions can substitute each other in a sense. The relationship can be described as: $1/b = 0.01c^2 + 0.11c + 0.24$ with R^2 higher than 0.96 at the monthly scale (Figure 5). The relationship keeps at other time scales with a slight difference in the regression coefficients. At the daily scale, when c is equal to 0, the corresponding b is equal to 4.5, which is the same as that of the theoretical derivation in Brutsaert (2015).

3.5 Uncertainty analysis

3.5.1 Influence of ecosystem types

The evaluation merits of the generalized complementary functions may differ among ecosystem types. However, our results show that such variation generally not affect our conclusion that the complementary functions perform best at the monthly scale. We show the performance of the two functions at multiple timescales for each ecosystem type in Table S2. Generally, the SGC function and the PGC function perform best at the monthly scale in most ecosystem types (9 of 11) with the highest NSE and R^2, which is consistent with the overall results. The exceptions include a closed shrubland site (CSH, N = 1) and evergreen broadleaf forests (EBF, N = 8), in which the complementary functions perform not as well as in other ecosystem types. The CSH site (IT-Noe) has the highest NSE_H (0.11) and NSE_B (0.12) at the annual scale. In the EBF group, the highest NSE_H (0.15) and NSE_B (0.03) occur at the weekly scale, but the R^2 values at the weekly scale ($R^2{}_H$ = 0.64; $R^2{}_B$= 0.62) and those at the monthly scale ($R^2{}_H$ = 0.62; $R^2{}_B$ = 0.61) are close. The RMSEs at the weekly scale are 14.95 W m^{-2} and 16.08 W m^{-2} for the sigmoid function and polynomial function, respectively, and those values at monthly scale are 12.36 W m^{-2} ($RMSE_H$) and 12.93 W m^{-2} ($RMSE_B$). We inferred the abnormal results of these two exceptions are related to the lower NSE values in these ecosystem types. The mean NSE values at multiple time scale of CSH (−0.75) and EBF (−0.66) are negative, while the values of the other ecosystem types are all positive.

3.5.2 Performance at seasonal scale

https://doi.org/10.5194/hess-2020-379
Preprint. Discussion started: 18 August 2020

In consideration of the substantial discrepancy between the monthly results and the annual results, we added an analysis at the seasonal scale, which is between the two timesteps. The relationship between the estimated E_{est} (site mean values) and the observed E of the 88 sites at seasonal scale is shown in Figure S1. For the SGC function, the regression result at the seasonal scale is similar to that at the monthly scale (Figure S1a and Figure 1c). The values of NSE_H (0.33), R^2_H (0.61), and $RMSE_H$ (10.16 W m^{-2}) at the seasonal scale are between the monthly results and the yearly results (Table 1). For the PGC functions, the regression result at the seasonal scale is extremely close to that at the yearly scale (Figure S1b and Figure 3d). The evaluation merits (NSE_B = 0.31; R^2_B = 0.63; $RMSE_B$ = 9.94 W m^{-2}) also range between the monthly results and the yearly results (Table 1). These results indicate that the decline of the model efficiency has already occurred at the seasonal scale and support our conclusion that the complementary functions perform best at the monthly scale.

3.5.3 Influence of energy balance residual correction methods

So far, there are mainly two methods for surface energy closure correction in the complementary studies. In the first method, the residual term is attributed into latent heat directly as the "energy residual" (ER) closure correction (e.g., Ershadi et al., 2014; Han and Tian 2018), which is adopted in above analysis. The second method is called the "Bowen ratio" (BR) closure correction, in which the residual term is attributed into sensible heat and latent heat by preserving Bowen ratio (e.g., Twine et al., 2000; Ma et al., 2015a). Based on different correction methods, the evaluation results of the model performance may differ. Thus, we recalculated our results by adopting the BR energy closure correction method. We

Hydrology and Earth System Sciences
Open Access
Discussions

found the mean value of 1/*b* changes from 0.29 ± 0.04 (ER) to 0.40 ± 0.05 (BR) and the mean value of *c* changes from −0.04 ± 0.23 (ER) to 0.63 ± 0.24 (BR) at monthly scale. It indicates the key parameters could be affected by adopting different correction methods. However, the results based on the BR method also support that the complementary functions perform best on evaporation estimation at monthly scale (Table 2). The NSE and R^2 vales increase from daily scale to monthly scale, and decrease from monthly scale to yearly scale, just following the pattern showed in Table 1. Generally, the evaluation results based on the BR method are worse than those based on the ER method. For example, when the ER method was replaced by the BR method the NSE and R^2 values decrease ($\Delta NSE_H = -0.15$; $\Delta NSE_B = -0.23$; $\Delta R^2_H = -0.07$; $\Delta R^2_B = -0.07$) and the RMSE values increase ($\Delta RMSE_H = 1.36$ W m^{-2}; $\Delta RMSE_B = 1.56$ W m^{-2}) at monthly scale. Ershadi et al. (2014) also found that the modeled E_{est} values by the PM equation, the AA approach and the modified Priestley-Taylor model (PT-JPL) show higher agreement with the ER corrected evaporation instead of the BR corrected evaporation. Ershadi et al. (2014) inferred the reason is that the observed sensible heat flux is more reliable than the observed latent heat flux. The measurement of latent heat by the EC tower may be confounded by minor instabilities when the boundary layer shrinks at night. To summarize, although the different energy closure correction methods have some influences on the key parameters and model efficiencies, they do not affect our conclusion that the generalized complementary functions perform best at monthly scale.

4. Conclusions

In this study, evaporation estimation was assessed over 88 EC monitoring sites at multiple

https://doi.org/10.5194/hess-2020-379
Preprint. Discussion started: 18 August 2020

Hydrology and Earth System Sciences
Discussions

time scales (daily, weekly, monthly, and yearly) by using two generalized complementary functions (the SGC function and the PGC function). The performance of the complementary functions at multiple time scales was compared, and the variation of the key parameters at different time scales was explored. The main findings are summarized as follows:

(1) The sigmoid and polynomial generalized complementary functions exhibit the highest skill in evaporation estimation at the monthly scale. The highest evaluation merits were obtained at this time scale. The accuracy of the complementary functions highly depends on the calculation timestep. The NSE increases from the daily scale (0.26, averaged by NSE_H and NSE_B) to the weekly scale (0.37) and monthly scale (0.53) while decreases at the seasonal scale (0.32) and the annual scale (0.22). The regression parameters between estimated E_{est} and observed site mean E also support this conclusion for the PGC function. The variations among different ecosystem types or between different energy balance correction methods generally have no effect on this conclusion. Further evaporation estimation studies by using the complementary functions can choose the monthly timestep to achieve the most accurate results.

(2) The SGC function and the PGC function are approximately identical under non-humid environments, while the SGC function performs better under super humid conditions implied by high values of x (> $1/\alpha$) when the PGC function is theoretically useless ($E_{est} > E_{pen}$). At daily and weekly time scales, quite a few ecosystems can experience frequent high x occurrences and thus the SGC function performs slightly better than the PGC function at

these time scales. However, they perform very similarly at monthly and annual time scales as few high x occurrences. Besides, the performance of the PGC function is more sensitive to the timestep than that of the SGC function.

(3) The key parameter b of the SGC function increases and the key parameter c of the PGC function decreased as time scale increases. The value of $1/b$ is a quadratic function of c with higher R^2 (> 0.96). The relationship at the monthly scale can be described as: $1/b = 0.01c^2 + 0.11c + 0.24$. It indicates the two functions can substitute each other to some extent.

In this study, in order to find the most suitable time scale for applying the complementary principle, the key parameters (b and c) were calibrated to achieve the best model performance at each timescale. Further studies on the prognostic application of the complementary principle could focus on the reasonable prediction of the key parameters, and with the predictable flexible parameters at different timescales, the complementary principle could be integrated into hydrological models to reduce the uncertainty associated with evaporation estimation.

Code/Data availability

All the data used in this study are from FLUXNET (http://fluxnet.fluxdata.org). The intermediate data are available on request from the corresponding author (tianfq@mail.tsinghua.edu.cn).

Author contribution

Songjun Han and Fuqiang Tian designed the experiments and Liming Wang carried them out. Liming Wang developed the model code and performed the simulations. Liming Wang prepared the manuscript with contributions from all co-authors.

Competing interests

The authors declare that they have no conflict of interest.

Acknowledgements

We are grateful for the financial support from National Science Foundation of China (NSFC 51825902, 51579249). We thank the scientists of FLUXNET (http://fluxnet.fluxdata.org) for their generous sharing of their eddy flux data.

References

Allen, R. G., Pereira, L. S., Raes, D., Smith, M.: Crop evapotranspiration: Guidelines for computing crop water requirements. FAO irrigation and drainage paper No. 56, Food and Agricultural Organization of the U.N., Rome, Italy, 1998.

Baldocchi, D., Falge, E., Gu, L., Olson, R., Hollinger, D., Running, S. et al.: FLUXNET: A new tool to study the temporal and spatial variability of ecosystem-scale carbon dioxide, water vapor, and energy flux densities. Bull Amer. Meteor. Soc., 82(11), 2415–2434, 2001. https://doi.org/10.1175/1520-0477(2001)082<2415:FANTTS>2.3.CO;2

Bouchet, R. J.: Evapotranspiration réelle et potentielle, signification climatique. IAHS Publ, 62, 134-142, 1963.

Brubaker, K. L., Entekhabi, D.: Analysis of feedback mechanisms in land-atmosphere interaction. Water Resour. Res., 32(5), 1343-1357, 1996. https://doi.org/10.1029/96wr00005

Brutsaert, W.: A generalized complementary principle with physical constraints for land-surface evaporation. Water Resour. Res., 51(10), 8087-8093, 2015. https://doi.org/10.1002/2015wr017720

Brutsaert, W.: Spatial distribution of global landscape evaporation in the early twenty first century by means of a generalized complementary approach. J. Hydrometeorol., 21(2), 287-298, 2019. https://doi.org/ 10.1175/JHM-D-19-0208.1

Brutsaert, W., Li, W., Takahashi, A., Hiyama, T., Zhang, L., Liu, W. Z.: Nonlinear advection-aridity method for landscape evaporation and its application during the growing season in the southern Loess Plateau of the Yellow River basin. Water Resour. Res., 53(1), 270-282, 2017. https://doi.org/ 10.1002/2016wr019472

Brutsaert, W., Parlange, M. B.: Hydrologic cycle explains the evaporation paradox. Nature, 396(6706), 30-30, 1998. https://doi.org/ 10.1038/23845

Brutsaert, W., Stricker, H.: Advection-Aridity approach to estimate actual regional evapotranspiration. Water Resour. Res., 15(2), 443-450, 1979. https://doi.org/ 10.1029/WR015i002p00443

Budyko, M.I.: Climate and life (Vol. 508). New York: Academic press, 1974.

Crago, R., Crowley, R.: Complementary relationships for near-instantaneous evaporation. J. Hydrol., 300(1-4), 199-211. https://doi.org/10.1016/j.jhydrol.2004.06.002, 2005.

Crago, R. D., Qualls, R. J.: Evaluation of the generalized and rescaled complementary evaporation relationships. Water Resour. Res., 54(10), 8086-8102, 2018. https://doi.org/10.1029/2018wr023401

Ershadi, A., McCabe, M. F., Evans, J. P., Chaney, N. W., Wood, E. F.: Multi-site evaluation of terrestrial evaporation models using FLUXNET data. Agric. For. Meteorol., 187, 46–61, 2014. https://doi.org/10.1016/j.agrformet. 2013.11.008

Fu, B. P.: On the calculation of the evaporation from land surface (in Chinese), Sci. Atmos. Sin., 5(1), 23 – 31, 1981.

Han, S. J., Hu, H. P., Tian, F. Q.: A nonlinear function approach for the normalized complementary relationship evaporation model. Hydrol. Processes, 26(26), 3973-3981, 2012. https://doi.org/10.1002/hyp.8414

Han, S. J, Hu, H. P., Tian, F. Q.: Evaluating the Advection-Aridity model of evaporation using data from field-sized surfaces of HEIFE. IAHS Publ., 322(2):9-14, 2008.

Han, S. J., Hu, H. P., Yang, D. W., Tian, F. Q.: A complementary relationship evaporation model referring to the Granger model and the advection-aridity model. Hydrol. Processes, 25(13), 2094-2101, 2011. https://doi.org/10.1002/hyp.7960

Han, S. J., Tian, F. Q.: Derivation of a sigmoid generalized complementary function for evaporation with physical constraints. Water Resour. Res., 54(7), 5050-5068, 2018.

https://doi.org/10.5194/hess-2020-379
Preprint. Discussion started: 18 August 2020

Hydrology and Earth System Sciences Discussions

https://doi.org/10.1029/2017wr021755

Han, S., Tian, F.: Complementary principle of evaporation: From original linear relationship to generalized nonlinear functions. Hydrol. Earth Syst. Sci., 24(5), 2269-2285, 2020. https://doi.org/10.5194/hess-24-2269-2020

Hobbins, M. T., Ramirez, J. A., Brown, T. C.: The complementary relationship in estimation of regional evapotranspiration: An enhanced Advection-Aridity model. Water Resour. Res., 37(5), 1389-1403, 2001. https://doi.org/10.1029/2000wr900359

Hobbins, M. T., Ramirez, J. A.: Trends in pan evaporation and actual evapotranspiration across the conterminous U.S.: Paradoxical or complementary? Geophys. Res. Lett. 31.13:405-407, 2004. https://doi.org/10.1029/2004GL019846

Hu, Z. Y., Wang, G. X., Sun, X. Y., Zhu, M. Z., Song, C. L., Huang, K. W., Chen, X. P.: Spatial-temporal patterns of evapotranspiration along an elevation gradient on Mount Gongga, Southwest China. Water Resour. Res., 54(6), 4180-4192, 2018. https://doi.org/10.1029/2018wr022645

Kahler, D. M., Brutsaert, W.: Complementary relationship between daily evaporation in the environment and pan evaporation. Water Resour. Res, 42(5), 2006. https://doi.org/10.1029/2005WR004541

Legates D. R., Mccabe G. J.: Evaluating the use of "goodness-of-fit" Measures in hydrologic and hydroclimatic model validation. Water Resour. Res., 35(1):233-241, 1999. https://doi.org/10.1029/1998wr900018

Liu, X. M., Liu, C. M., Brutsaert, W.: Regional evaporation estimates in the eastern monsoon region of China: Assessment of a nonlinear formulation of the complementary principle. Water Resour. Res., 52(12), 9511-9521, 2016. https://doi.org/10.1002/2016wr019340

Ma, N., Szilagyi, J., Zhang, Y., Liu, W.: Complementary relationship-based modeling of terrestrial evapotranspiration across China during 1982–2012: Validations and spatiotemporal analyses. J. Geophys. Res. Atmos., 124, 4326–4351, 2019. https://doi.org/10.1029/2018JD029850

Ma, N., Zhang, Y. S., Szilagyi, J., Guo, Y. H., Zhai, J. Q., Gao, H. F.: Evaluating the complementary relationship of evapotranspiration in the alpine steppe of the Tibetan Plateau. Water Resour. Res., 51(2), 1069-1083, 2015a. https://doi.org/10.1002/2014wr015493

Ma, N., Zhang, Y. S., Xu, C. Y., Szilagyi, J.: Modeling actual evapotranspiration with routine meteorological variables in the data-scarce region of the Tibetan Plateau: Comparisons and implications. J. Geophys. Res. Biogeosci., 120(8), 1638-1657, 2015b. https://doi.org/10.1002/2015jg003006

Monin, A., Obukhov, A.: Basic laws of turbulent mixing in the surface layer of the atmosphere. Contrib. Geophys. Inst. Acad. Sci. USSR, 151(163), e187, 1954.

Monteith, J. L.: Evaporation and environment (pp. 205-234): Paper presented at the Symposia of the society for experimental biology. Cambridge University Press (CUP) Cambridge, 1965.

Morton, F. I.: Operational estimates of areal evapo-transpiration and their significance to the science and practice of hydrology. J. Hydrol., 66(1-4), 1-76, 1983. https://doi.org/10.1016/0022-1694(83)90177-4

Neelin, J. D., Held, I. M., Cook, K. H.: Evaporation-wind feedback and low-frequency variability in the tropical atmosphere. J. Atmos. Sci., 44(16), 2341-2348, 1987. https://doi.org/ 10.1175/1520-0469(1987)044<2341:Ewfalf>2.0.Co;2

Parlange, M. B., Katul, G. G.: An advection-aridity evaporation model, Water Resour. Res., 28, 127-132, 1992. https://doi.org/10.1029/91WR02482

Penman, H. L.: The dependence of transpiration on weather and soil conditions. J. Soil Sci., 1(1), 74-89, 1950. https://doi.org/10.1111/j.1365-2389.1950.tb00720.x

Penman, H. L.: Natural evaporation from open water, bare soil and grass. Proc. R. Soc. London, Ser. A., 193(1032), 120-145, 1948. https://doi.org/10.1098/rspa.1948.0037

https://doi.org/10.5194/hess-2020-379
Preprint. Discussion started: 18 August 2020

Priestley, C. H. B., Taylor, R. J.: On the assessment of surface heat-flux and evaporation using large-scale parameters. Mon. Weather Rev., 100(2), 81-92, 1972. https://doi.org/10.1175/1520-0493(1972)100<0081:Otaosh>2.3.Co;2

Qualls, R. J., Gultekin, H.: Influence of components of the advection-aridity approach on evapotranspiration estimation. J. Hydrol., 199(1-2), 3-12, 1997. https://doi.org/10.1016/S0022-1694(96)03314-8

Shukla, J., Mintz, Y.: Influence of land-surface evapo-transpiration on the earths climate. Science, 215(4539), 1498-1501, 1982. https://doi.org/10.1126/science.215.4539.1498

Twine, T. E., Kustas, W. P., Norman, J. M., Cook, D. R., Houser, P., Meyers, T. P., Wesely, M. L.: Correcting eddy-covariance flux underestimates over a grassland. Agric. For. Meteorol., 103(3), 279-300, 2000. https://doi.org/10.1016/S0168-1923(00)00123-4

Wang, K. C., Dickinson, R. E.: A review of global terrestrial evapotranspiration: observation, modeling, climatology, and climatic variability. Rev. Geophys., 50, 2012. https://doi.org/10.1029/2011rg000373

Wang, L.M., Tian, F. Q., Han, S. J., Wei, Z. W.: Determinants of the asymmetric parameter in the generalized complementary principle of evaporation. Water Resour. Res, 2020 (accepted). https://doi.org/10.1029/2019WR026570

Zhang, L., Cheng, L., Brutsaert, W.: Estimation of land surface evaporation using a generalized nonlinear complementary relationship. J. Geophys. Res. Atmos., 122(3), 1475-1487, 2017. https://doi.org/10.1002/2016jd025936

Zhou, H., Han, S., Liu, W.: Evaluation of two generalized complementary functions for annual evaporation estimation on the loess plateau, china. J. Hydrol., 587, 124980, 2020. https://doi.org/10.1016/j.jhydrol.2020.124980

https://doi.org/10.5194/hess-2020-379
Preprint. Discussion started: 18 August 2020

List of Figure Captions

Figure 1. The estimated evaporation based on the SGC function (equation (1)) vs the observed site mean evaporation at the daily scale (a), weekly scale (b), monthly scale (c) and yearly scale (d). Each dot represents the site mean result (N = 88 in each panel). The regression equations and determination coefficients (R^2) were calculated by the site mean results of the 88 EC sites.

Figure 2. Plots of E/E_{pen} with respect to $E_{\mathrm{rad}}/E_{\mathrm{pen}}$ for five selected sites at multiple time scales. The black dots represent the observations; the red lines represent the SGC function; the green lines represent the PGC function; the blue lines are the P-T and Penman boundary lines. ENF, evergreen needleleaf forests; DBF, deciduous broadleaf forests; WSA, woody savannas; CRO, croplands; GRA, grasslands.

Figure 3. As in Figure 1 except for PGC function (equation (5)).

Figure 4. Plots of the SGC equation (1) with α = 1.26 and varying $1/b$ values at multiple time scales (a). Plots of the PGC equation (5) with α = 1.26 and varying c values at multiple time scales (b). The blue lines are the P-T and Penman boundary lines.

Figure 5. Distribution of the key parameter $1/b$ at daily scale (a), weekly scale (b), monthly scale (c) and yearly scale (d): EBF, evergreen broadleaf forests (8); ENF, evergreen needleleaf forests (27); DBF, deciduous broadleaf forests (13); MF, mixed forests (5); Shrub (12), closed shrubland, open shrublands, woody savannas and savannas; CRO, croplands (6); WET, permanent wetlands (2).

Figure 6. Distribution of the key parameter c at daily scale (a), weekly scale (b), monthly scale (c) and yearly scale (d): EBF, evergreen broadleaf forests (8); ENF, evergreen

https://doi.org/10.5194/hess-2020-379
Preprint. Discussion started: 18 August 2020

needleleaf forests (27); DBF, deciduous broadleaf forests (13); MF, mixed forests (5); Shrub (12), closed shrubland, open shrublands, woody savannas and savannas; CRO, croplands (6); WET, permanent wetlands (2).

Figure 7. Relationships between $1/b$ and c at the monthly scale.

Table 1. The evaluation merits (NSE, R^2 and RMSE in W m^{-2}) of the two generalized complementary functions using the "energy residual" (ER) closure correction method. The subscript H and B correspond to the SGC function proposed in Han and Tian (2018) and the PGC function proposed in Brutsaert (2015), respectively.

	Day	Week	Month	Season	Year
NSE_H	0.33	0.44	0.55	0.33	0.18
NSE_B	0.19	0.3	0.50	0.31	0.25
R^2_H	0.62	0.7	0.74	0.61	0.61
R^2_B	0.61	0.7	0.75	0.63	0.63
$RMSE_H$	24.56	17.67	13.20	10.16	7.33
$RMSE_B$	26.83	19.17	13.70	9.94	6.96

Table 2. The evaluation merits (NSE, R^2 and RMSE in W m^{-2}) of the two generalized complementary functions using the "Bowen ratio" (BR) closure correction method. The subscript H and B correspond to the SGC function proposed in Han & Tian (2018) and the PGC function proposed in Brutsaert (2015), respectively.

	Day	Week	Month	Season	Year
NSE_H	0.01	0.23	0.4	0.17	−0.07
NSE_B	−0.28	0.03	0.27	0.11	−0.23
R^2_H	0.53	0.62	0.67	0.54	0.52
R^2_B	0.52	0.61	0.68	0.55	0.52
$RMSE_H$	26.62	18.9	14.56	11.3	7.88
$RMSE_B$	29.77	20.59	15.26	11.3	8.03

https://doi.org/10.5194/hess-2020-379
Preprint. Discussion started: 18 August 2020

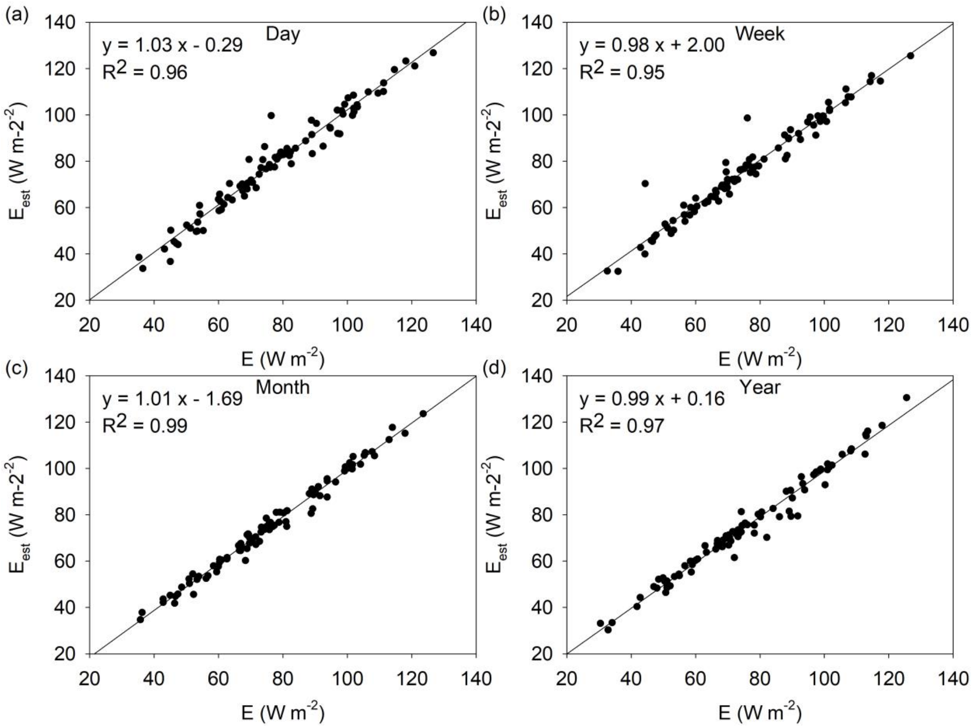

Figure 1. The estimated evaporation based on the SGC function (equation (1)) vs the observed site mean evaporation at the daily scale (a), weekly scale (b), monthly scale (c) and yearly scale (d). Each dot represents the site mean result (N = 88 in each panel). The regression equations and determination coefficients (R^2) were calculated by the site mean results of the 88 EC sites.

https://doi.org/10.5194/hess-2020-379
Preprint. Discussion started: 18 August 2020

Hydrology and Earth System Sciences
Open Access
Discussions

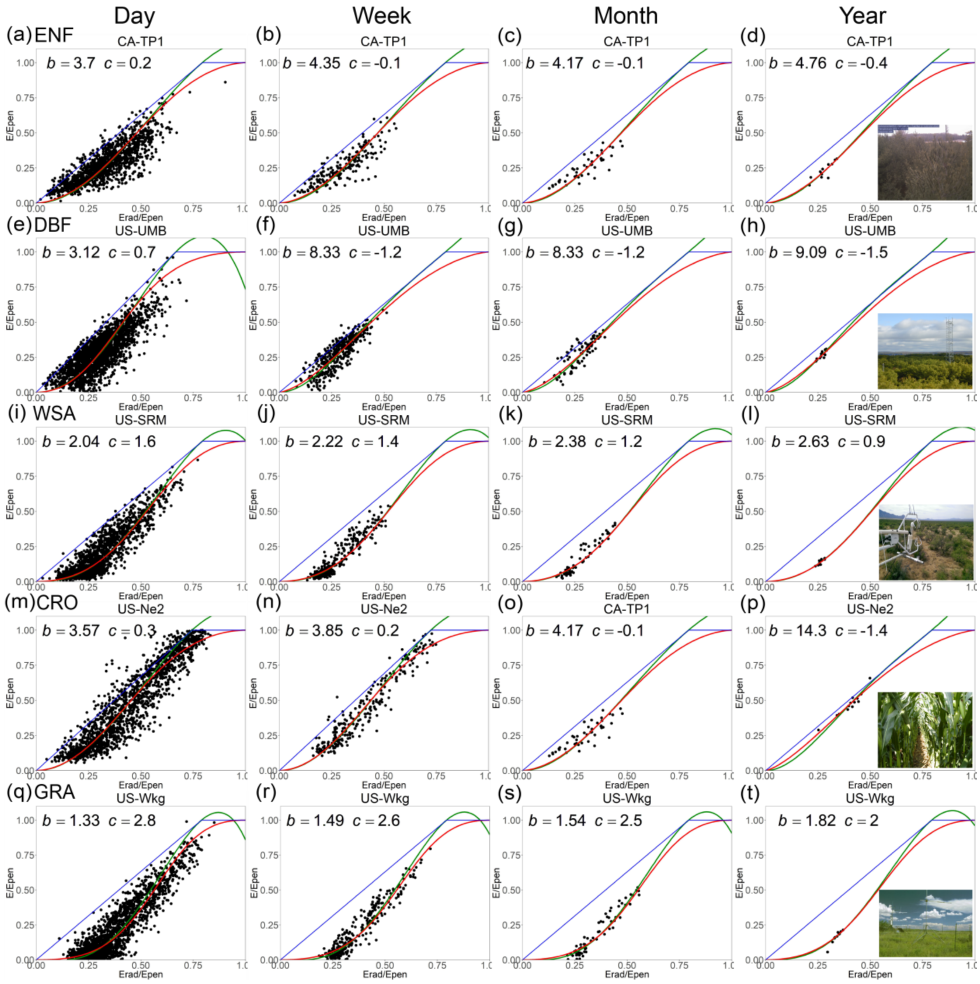

Figure 2. Plots of E/E_{pen} with respect to E_{rad}/E_{pen} for five selected sites at multiple time scales. The black dots represent the observations; the red lines represent the SGC function; the green lines represent the PGC function; the blue lines are the P-T and Penman boundary lines. ENF, evergreen needleleaf forests; DBF, deciduous broadleaf forests; WSA, woody savannas; CRO, croplands; GRA, grasslands.

https://doi.org/10.5194/hess-2020-379
Preprint. Discussion started: 18 August 2020

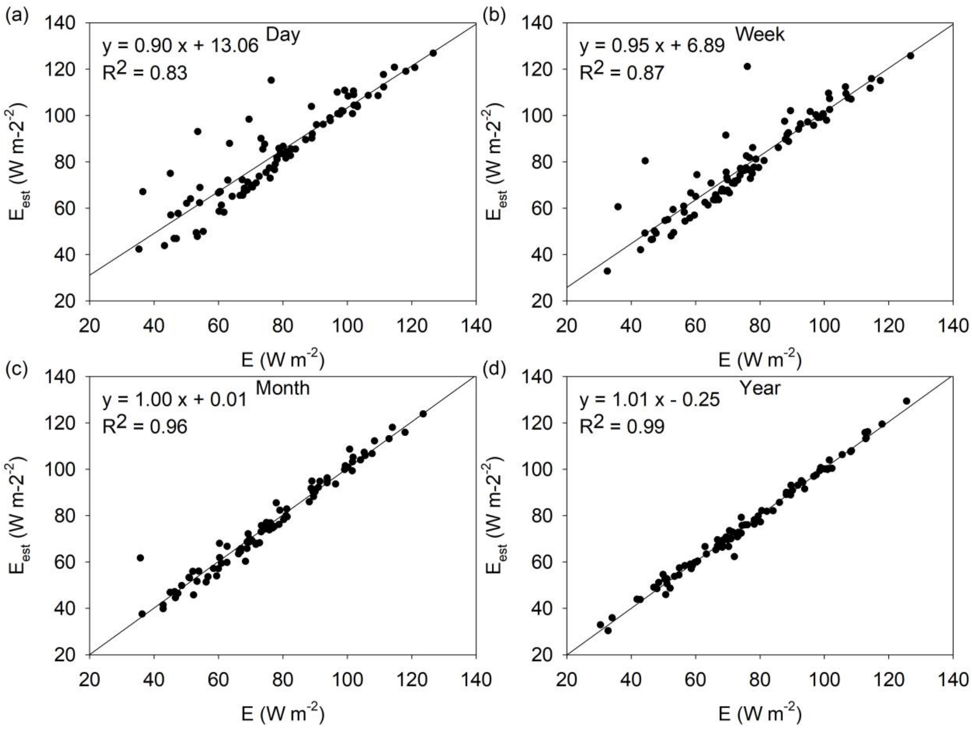

Figure 3. As in Figure 1 except for PGC function (equation (5)).

https://doi.org/10.5194/hess-2020-379
Preprint. Discussion started: 18 August 2020

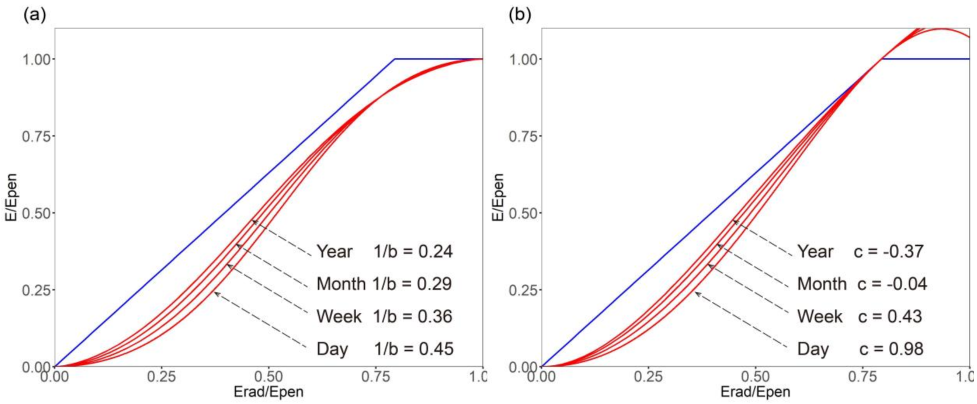

Figure 4. Plots of the SGC equation (1) with α = 1.26 and varying 1/b values at multiple time scales (a). Plots of the PGC equation (5) with α = 1.26 and varying c values at multiple time scales (b). The blue lines are the P-T and Penman boundary lines.

https://doi.org/10.5194/hess-2020-379
Preprint. Discussion started: 18 August 2020

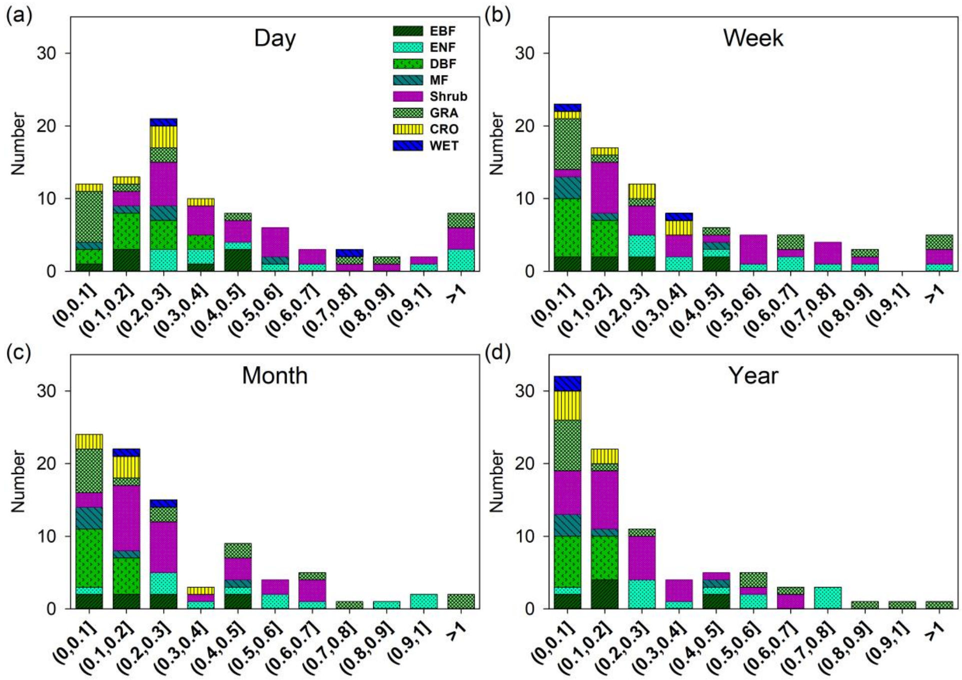

Figure 5. Distribution of the key parameter 1/*b* at daily scale (a), weekly scale (b), monthly scale (c) and yearly scale (d): EBF, evergreen broadleaf forests (8); ENF, evergreen needleleaf forests (27); DBF, deciduous broadleaf forests (13); MF, mixed forests (5); Shrub (12), closed shrubland, open shrublands, woody savannas and savannas; CRO, croplands (6); WET, permanent wetlands (2).

Hydrology and Earth System Sciences
Open Access
Discussions

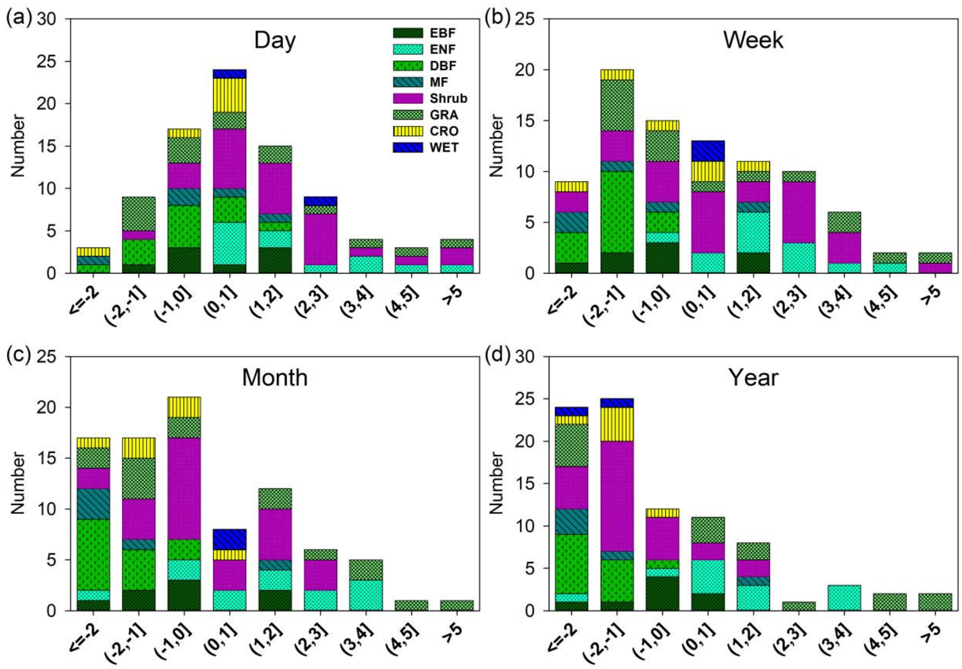

Figure 6. Distribution of the key parameter *c* at daily scale (a), weekly scale (b), monthly scale (c) and yearly scale (d): EBF, evergreen broadleaf forests (8); ENF, evergreen needleleaf forests (27); DBF, deciduous broadleaf forests (13); MF, mixed forests (5); Shrub (12), closed shrubland, open shrublands, woody savannas and savannas; CRO, croplands (6); WET, permanent wetlands (2).

https://doi.org/10.5194/hess-2020-379
Preprint. Discussion started: 18 August 2020

Hydrology and Earth System Sciences
Discussions

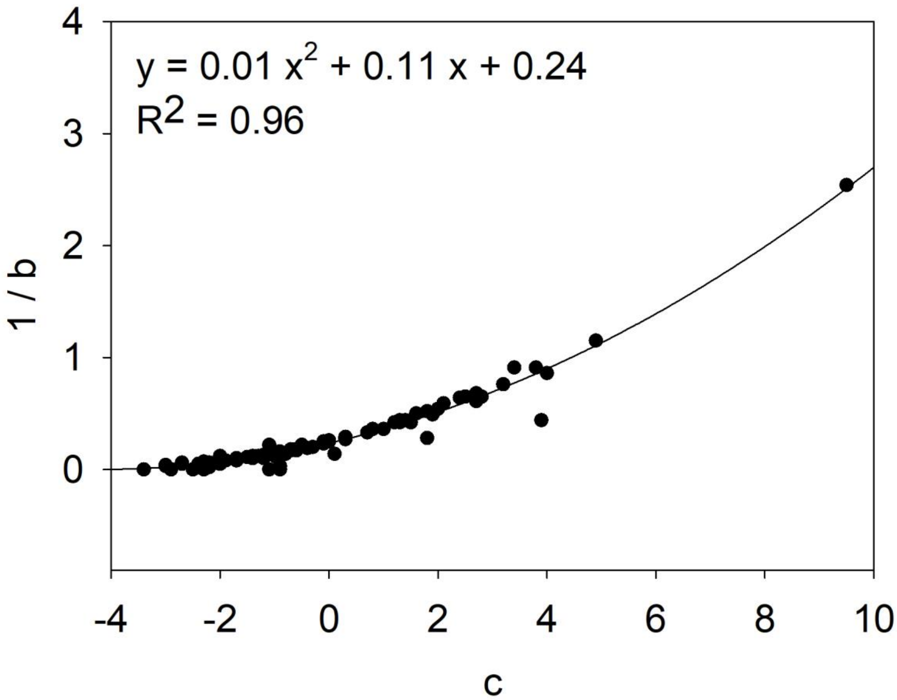

Figure 7. Relationships between 1/*b* and *c* at the monthly scale.